Visible Channel Calibration on GOES Imagers using Venus and Moon

KIGAWA Seiichiro*

Abstract

Venus is the brightest planet that can be observed from geostationary orbit. The brightness of Venus is suitable for the visible channel calibration of an imaging instrument, although there is a concern about the stability of the brightness due to clouds on Venus. The moon is relatively dark, and the available albedo range of calibration by the moon is limited to a lower albedo region. However, the moon has no atmosphere, and its surface is stable enough to provide information on the visible channel calibration.

A new technique for on-orbit visible channel calibration using Venus and the moon was developed. Venus works as a calibration reference at high albedo, and the moon at low. The Apollo 16 landing site on the moon was selected for the calibration reference because the laboratory-measured soil reflectance of the landing site is available. It was estimated that the sensitivity of the visible channel of GOES-9 Imager in April 2004 was 59 percent of the pre-launch measurement at the low albedo region. The non-linearity (i.e., a meaningful quadratic term of a calibration equation) was found in the sensitivity of the visible channel. The estimation is verified by Jupiter's brightness and by cloud brightness on the earth.

1. Introduction

A visible channel is a long-established channel of an imaging instrument operated on geostationary orbit. It has been used since 1974 by the SMS-1 (Synchronous Meteorological Satellite) and provides useful information on the troposphere and land/sea surface. Although visible light is the light that is closest to us, the instrumental calibration of the visible channel on weather satellites is not always quantitative, because it is not easy to install a cumbersome visible calibration device in the instruments. Sunlight is used to calibrate the instrument, but it is not full-aperture calibration, and large uncertainty exists on the mechanism that introduces the sunlight into the instrument. Various studies have been conducted, such as inter-sensor comparison of earth scenes, and measurement of sensor degradation using a radiometrically stable ground site like a dry desert. However, the earth is the object of observation, so these should be defined as the verification of the calibration, not the calibration itself. At least, it is desired that the calibration reference should be found outside of the earth.

In May 2003, Geostationary Operational Environmental Satellite (GOES)-9, operated by the National Oceanic and Atmospheric Administration (NOAA), started contingency backup operations at 155 degrees East longitude for the aged Japanese Geostationary Meteorological Satellite (GMS)-5. The source of all the imager products generated by the Meteorological Satellite Center was switched from GMS-5 to GOES-9. Because GOES-9 has no device to calibrate the visible channel of the Imager, it was desired to know the latest calibration information on the visible channel based on the imagery itself, and that was the motivation of this study.

* Meteorological Satellite Center, Office of Preperation for Meteorological Satellite Operations
Received November 18, 2004 Revised February 1, 2005

2. Visible Calibration using the Moon and Planets

Venus is the brightest planet that can be detected by the Imager. Figure 1 shows a part of the GOES-12 visible channel imagery taken on February 21, 2004, 0815 UT, which contains Venus near the limbs of the earth. Venus rarely appeared in the imagery and the time zone of its presence is limited to around local midnight. The brightness of Venus is enough to apply to the visible channel calibration, but there is a concern about the stability of the brightness, because Venus has an atmosphere with some clouds.

The moon has no atmosphere, and its surface is stable enough for the visible calibration. There is a reflectance analysis of the lunar soil that was brought back to the earth by the Apollo missions. However, the moon is relatively dark, and the available albedo range of calibration by the moon is limited into a lower albedo region. Figure 2 gives a view of the moon located near the limbs of the earth, taken on March 6, 2004, at 2100 UT, just at local noon. The moon gives useful information on the visible calibration around local noon, in contrast to Venus, when the visible channel is most informative.

The third astronomical object is Jupiter, as shown in Figure 3. Although Jupiter is darker than the moon on the GOES imagery, and it has an atmosphere with varied clouds, Jupiter appears in the imagery more frequently at both noon and midnight, so that it is expected to have a supplementary role.

A combination of Venus and the moon is the best approach to calibrate on-orbit instruments. Venus brings a calibration point at high albedo, and the moon at low, so that information on the linearity of the visible channel response can be obtained.

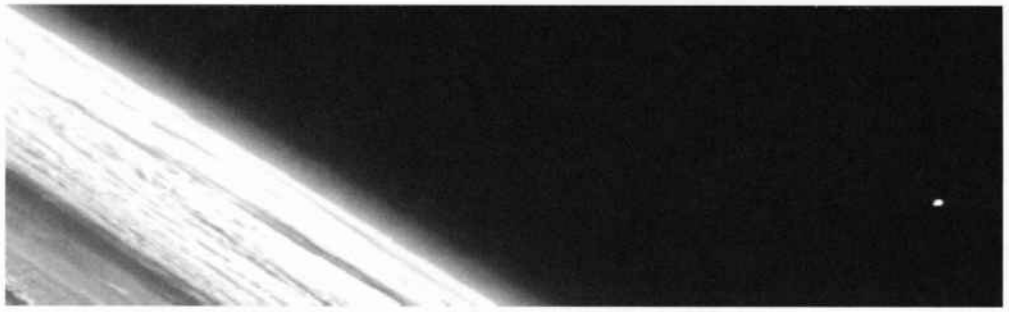

Figure 1. View of Venus and the Earth

Captured by GOES-12 on February 21, 2004, 0815 UT. Venus can be found on the right side of the imagery as a bright dot. Venus is the brightest planet that can be observed from geostationary weather satellites except for the earth.

Figure 2. View of the Moon and the Earth

Captured by GOES-10 on March 6, 2004, 2100 UT. This imagery is compensated to remove the motion of the moon during Imager's scanning and is enhanced so it can be easily seen. The moon has no atmosphere, and its surface changes are extremely slow, so that the moon is the most reliable as a calibration reference.

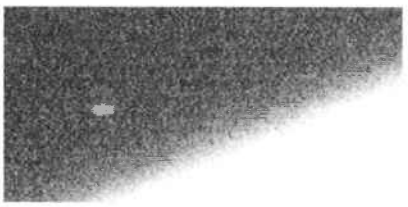

Figure 3. View of Jupiter and the Earth
Captured by GOES-10 on February 23, 2130 UT. Because Jupiter is very dark as compared with Venus, the earth is saturated.

3. Calibration by Venus

Venus has moderate brightness and a visual angle: Venus is brighter than the moon, its brightness is not saturated in observed digital counts, and the size of Venus on an image is larger than one pixel. Venus appears in the GOES imagery as a superb dot that is enough for calibration use. Figure 4 shows enlarged images of Venus taken by three GOES satellites on the same day. It can be seen from the figure that the Venus image captured by GOES-10 (middle photo) is darker than those captured by GOES-9 and -12. This observation is confirmed by Figure 5, that shows GVAR (GOES Variable) counts. These counts originated in Venus, but the width of the Venusian pixels on the GOES-10 imagery is wider than the others, that is, it seems that they are caused by the wide field-of-view of a pixel.

Figure 6 gives a graphical representation of the visible calibration by Venus. The observed pixel counts are interpolated using a sinc function defined by sinc (x) = sin (π x) / (π x). The astronomical information on Venus such as the brightness and distance was calculated by an ephemeris (e.g., Rika nenpyo: Chronological Scientific Tables), and then the information gives a predicted Venus image. The field of view of a pixel is measured at the east and south edges of Venus using the observed image, and then the field of view is used to generate the predicted Venus image. The measured field of view is shown in Figure 7. It is clear from this figure that GOES-10 has a wide field of view, as expected in the above. The wide field of view on GOES-10 is probably not permanent, because the solar illumination of a scan mirror of GOES-10 Imager was different from GOES-9 and 12, due to the yaw-flip mode (i.e., upside-down orientation in the north-south direction) on GOES-10, even if the geometry of the Sun-Venus-satellite is the same among the three satellites.

Comparison between the observed and predicted images verifies the validity of the predicted image. Figure 8 shows the GVAR counts of the observed Venus image in the vertical axis and the predicted image in the horizontal axis. Figure 8 indicates that the predicted brightness generated by the ephemeris is close to the observed brightness, although some errors exist, due to incomplete field-of-view measurements because of no oversampling in the north-south direction and visible channel detector noise.

The Venus-based calibration is given by a comparison of the maximum brightness between the observed and predicted images as listed in Table 1. The GOES constellation: GOES-9, 10, and 12 took 14, 4, and 6 images of Venus in early 2004. Only the observation of a single scan case, that is, Venus located in one scan of the eight visible channel detectors, is listed in Table 1. Note that the ephemeris used to generate the predicted brightness was a prediction, not an actual measurement by an astronomical observatory. The error of the predicted brightness, including the effect of the Venusian clouds, is discussed in Section 6.

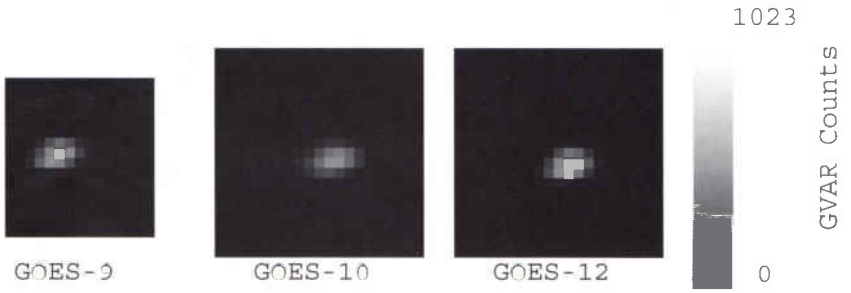

Figure 4. Comparison of Venus observed by GOES satellites

Venus was observed by the GOES constellation on February 25, 2004. The imaging times of GOES-9, 10, and 12 were 1613, 1130, and 0815 UT, respectively.

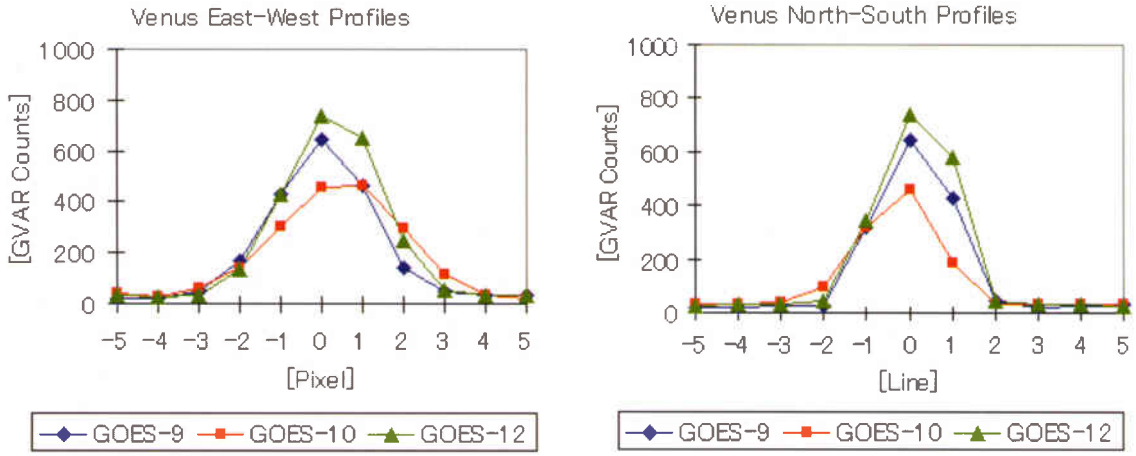

Figure 5. GVAR Counts of Venus

These figures show the GVAR counts that originated in Venus in both east-west and north-south directions, centered on the brightest pixel of Venus.

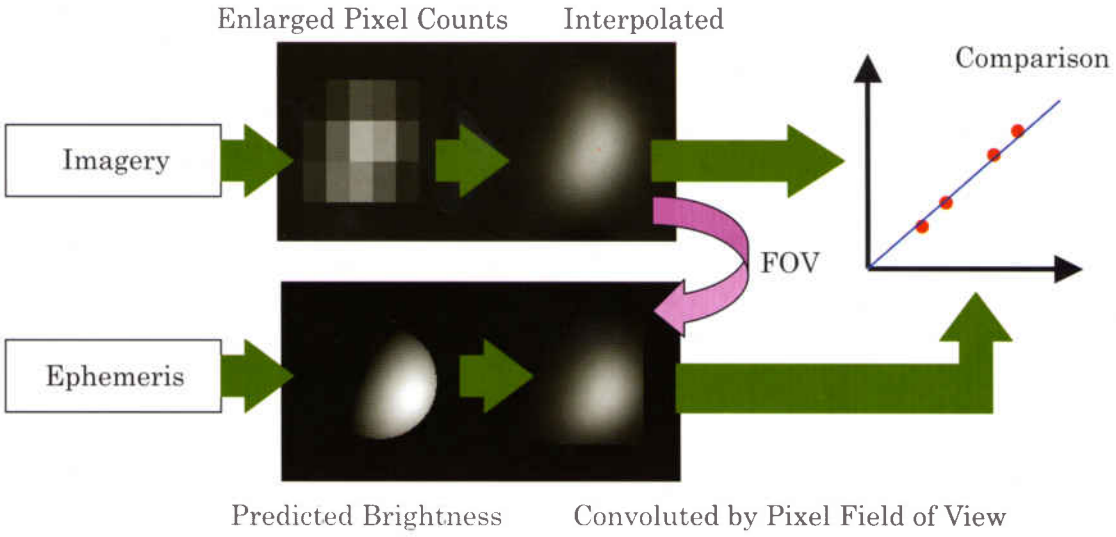

Figure 6. Schematic Diagram of Visible Calibration using Venus

The field of view of a pixel is estimated from an interpolated image at the east and south edges in this case. The interpolated imagery is compared with the convoluted brightness prediction on an East-West line that contains the brightest point.

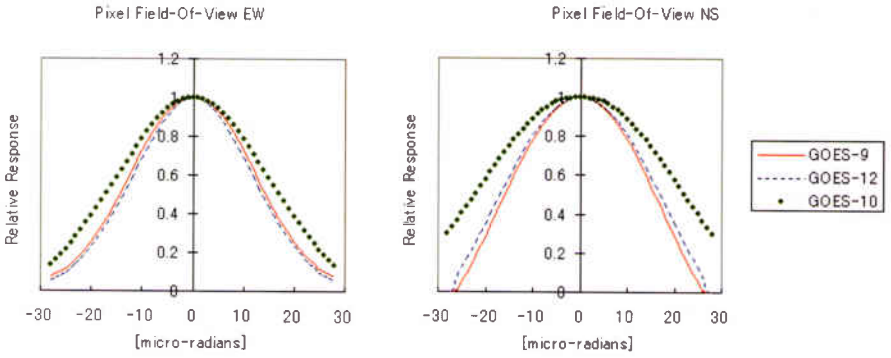

Figure 7.　Measured Field of View of Three GOES Imagers

Field-of-view measurement in the North-South direction (right graph) is not perfect, because there is no over-sampling in the North-South direction, and some higher spatial frequency information is lost.

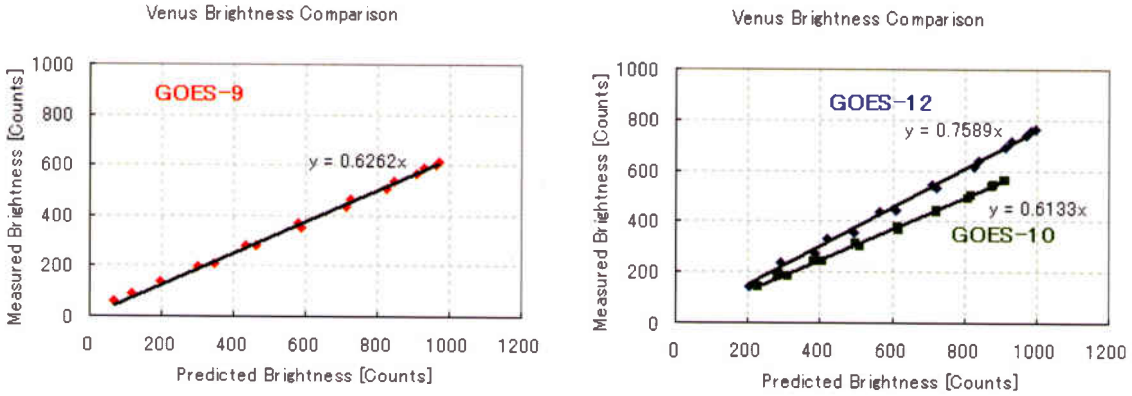

Figure 8.　Comparison of Venus Brightness

The Venus image taken on February 24 is used for GOES-9, that of February 2 for GOES-10, and that of February 25 for GOES-12.　The points of this comparison are selected on an East-West line that contains the brightest point.

Satellite	Date	Time [UT]	Maximum brightness [GVAR counts]		O / C	O / C mean
			Observed (O)	Predicted (C)		
9	01-24-2004	1525	726	953	0.754*	
9	01-24-2004	1613	723	1145	0.622*	
9	01-26-2004	1525	693	1105	0.617*	
9	01-27-2004	1525	690	990	0.688*	
9	01-29-2004	1525	685	1134	0.593*	
9	01-30-2004	1525	719	1128	0.628	0.630
9	01-31-2004	1525	687	1066	0.634	
9	02-24-2004	1613	664	1040	0.628	
9	02-25-2004	1613	653	940	0.629*	
10	02-02-2004	1200	567	940	0.591	0.583
10	02-25-2004	1130	516	879	0.574	
12	02-21-2004	0815	782	1046	0.740	0.748
12	02-23-2004	0815	780	1066	0.724	
12	02-24-2004	0732	830	1067	0.771	
12	02-25-2004	0815	789	1035	0.756	

Table 1. Maximum Brightness of Venus

*: Venus located on noisy detectors. The periodic noise of GOES-9 significantly affects this estimation, because the noise is sine-shaped.

4. Calibration by Lunar Reference

The landing site of Apollo 16 on the moon was used as the calibration reference because of the availability of soil reflectance information. This site was used to calibrate the Clementine mission data (Pieters, 1999) and the reflectance of the soil captured at the landing site was measured at the ground laboratory as a function of wavelength. This soil reflectance information has no uncertainty caused by observing it through the atmosphere, like ground-based observation. The landing site on the visible imagery was positioned by the use of four albedo features: Aristarchus, Menelaus, Proclus and Tycho shown in Figure 9. The albedo features work as lunar landmarks to calculate the position of the Apollo 16 landing site on the imagery.

Figure 10 shows the lunar images that were used to estimate the visible calibration information for GOES-9. There were more chances to capture the moon for GOES-9, rather than GOES-10 and 12, because of the full-disk-basis observation schedule on GOES-9. The Apollo 16 landing site was found on these images, and then the albedo value of the site was calculated using pre-launch calibration coefficients, and the averaged GVAR counts of 3 by 3 pixels. The measured albedo value was converted to the equivalent value at the standard geometry that has the same incident and reflected angles as the laboratory measurements (the incident angle was 30 degrees, and reflected angle 0). The laboratory measurements are used as a Bi-directional Reflectance (Scattering) Distribution Function. The conversion of the albedo value from measured to standard is given by

$$Cs = C \cdot \frac{\cos(30°) \cdot \cos(\theta sat)}{\cos(\theta sun)} \cdot D^2 \qquad (1)$$

where

Cs : Albedo value of standard geometry

C : Measured albedo value

θsun : Solar zenith angle at Apollo 16 landing site

θsat : Satellite zenith angle at Apollo 16 landing site

D : Sun-earth distance in the astronomical unit

Two of nine cases are selected, as shown in Table 2, to compare the albedo value with laboratory-measured reflectance directly, because of a smaller azimuthal difference, as a similar photometric condition to the laboratory measurement. The average of two cases give the standard geometry albedo of 0.0925. On the other han the lunar "ground-truth" albedo of the landing site that was calculated by the spectral response of the visible channel and the spectral reflectance of Apollo 16 soil 62231 was 0.1577. Hence, it is estimated that the sensitivity of the visible channel in April 2004 was 0.0925/0.1577 = 0.587 of pre-launch measurement.

The geometry of the sun, moon and satellite is not always suitable for comparison with the laboratory reflectance measurement. As shown in Table 2, more cases have a larger azimuth angle difference between the sun and satellite; hence an additional photometric correction should be developed based on empirical knowledge, not theoretical. From geostationary satellites, the moon is 10 times as far away as the earth, so that the spatial resolution of the visible channel is about 10 km on the lunar surface. Because an area of about 100 square kilometers must have many craters and undulations, the measured albedo cannot be interpreted by only the laboratory-measured reflectance, especially at a large phase angle region. Actually, the measured albedo of the standard geometry is dependent on a phase angle (i.e., a separation angle between the sun and satellite on the lunar surface) as shown in Figure 11. Because the moon imagery used for this technique is limited to around satellite local noon to ensure success in finding the lunar landmarks, the zenith angle of both the sun and satellite at the landing site is almost limited to 30 degrees. Therefore the difference of an azimuth angle between the sun and satellite at the landing site is a major contributor for the brightness, and then the effect of the phase angle can be expressed by a relatively simple function, as shown in Figure 11. Finally, the additional photometrical correction is introduced as the inverse of a polynomial function shown in Figure 11. The correction is given by

$$Cp = Cs \cdot \frac{0.587 \times 0.1577}{0.1173 - 3.018 \times 10^{-3}\theta + 3.399 \times 10^{-5}\theta^2} \qquad (2)$$

where

Cp : Photometrical-corrected albedo

θ : Phase angle [degree]

Because the photometrical correction is not dependent on the instrument, the photometrical-corrected albedo of both GOES-10 and 12 can be estimated, as shown in Table 3. It is estimated that the ratio of the sensitivity in April 2004 to the pre-launch measurement is 0.57 for GOES-10, and 0.68 for GOES-12.

The sensitivity ratio for GOES-9 and 10 can be compared with star-based responsivity trending analysis (Chang et al., 2004), which shows a relative responsivity of 0.57 for GOES-9 and 0.64 for GOES-10.

The above-mentioned approach is based on only space-borne information, that is, the lunar ground truth reflectance and the photometrical correction produced by GOES-9 observations. Though uncertainty remains in the photometrical correction due to lack of data, it must be improved by the analysis of archival imager data and additional chances to capture the moon in the future.

Figure 9. Lunar Landmarks

Four bright features: Aristarchus, Menelaus, Proclus and Tycho are used as lunar landmarks to know where the Apollo 16 landing site is on the imagery.

Figure 10. GOES-9 Lunar Images used for Visible Channel Calibration

Lunar images of various phase angles and distances have been obtained around local noon. Since periodic noise exists in the GOES-9 visible channel, the noise filter based on a bandpass digital filter is applied to the images.

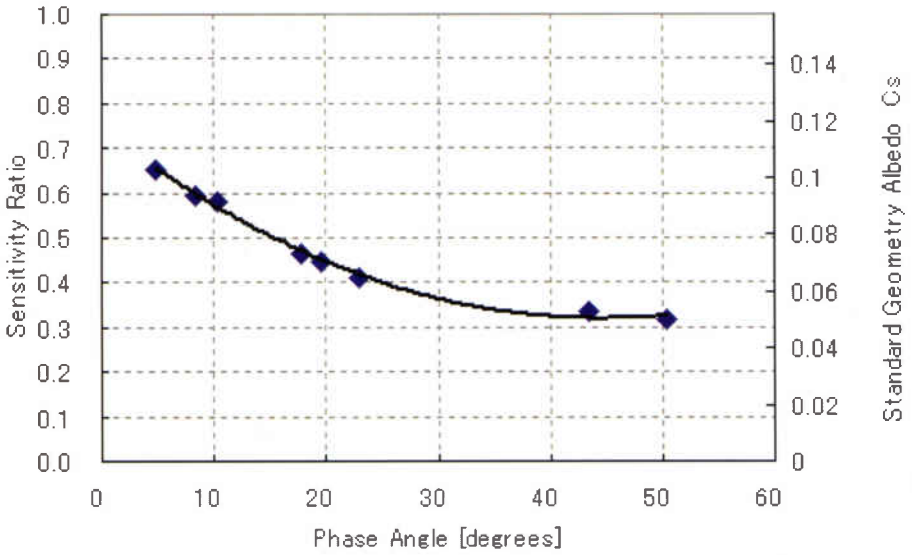

Figure 11. GOES-9 Lunar Albedo at Apollo 16 Landing Site Standard Geometry

The degradation rate, 5.4% per year, given by star-based responsivity trending analysis (Chang et al., 2004) was applied to calculating the standard geometry albedo shown in this figure. A factor is calculated by the degradation rate and the number of days from April 6, 2004, which compensates for the standard geometry albedo.

Date	Time [UT]	Phase angle [deg]	Azimuth Difference [deg]	Measured Albedo (C)	Standard Geometry Albedo (Cs)	Laboratory-Measured Albedo (CL)	Cs / CL
10-11-2003	02:26	10.3	20	0.104	0.092		
11-06-2003	23:29	23.0	103	0.079	0.065		
03-07-2004	02:25	4.8	7	0.118	0.103		
04-06-2004	01:50	8.3	1	0.101	0.093	0.1577	0.59
04-06-2004	02:50	10.3	2	0.098	0.092	0.1577	0.58
04-30-2004	22:51	50.4	157	0.054	0.050		
05-30-2004	23:14	43.4	136	0.056	0.053		
09-26-2004	23:49	19.6	70	0.081	0.071		
09-27-2004	00:48	17.6	65	0.083	0.073		

Table 2. GOES-9 Lunar Geometry and Albedo

A phase angle is defined by the separation angle between the sun and satellite viewing from the lunar surface. An azimuth difference angle is the difference of azimuth between the sun and satellite. Two images taken on April 6 gave a chance to know a key parameter: the ratio of the standard geometry albedo to the laboratory-measured reflectance.

Sat	Date	Time [UT]	Phase angle [deg]	Azimuth Difference [deg]	Measured Albedo (C)	Corrected Albedo (Cp)	Laboratory-Measured Albedo (CL)	Cp / CL
10	03-06-2004	21:00	3.3	8	0.123	0.090*	0.160	0.56
10	08-30-2004	21:20	11.2	22	0.0904	0.091*	0.160	0.57
10	09-29-2004	21:33	16.6	40	0.0789	0.091*	0.160	0.57
12	05-03-2004	15:10	17.6	40	0.1086	0.109*	0.160	0.68
12	08-30-2004	18:07	10.9	28	0.114	0.109*	0.160	0.68

Table 3. Photometrical-corrected Lunar Albedo of GOES-10 and 12

As expected, the moon works as one stable calibration reference.

*: Photometrical correction given by Equation 2 is applied to the standard geometry albedo.

5. Calibration Corrections

Venus gives a calibration point at high albedo, and the moon at low albedo. The ratio of the observed Venusian and lunar brightness to the predicted brightness, that is, the ratio of Imager sensitivity to the pre-launch calibration, is summarized in Table 4. It is clear from Table 4 that Venus shows a different ratio from the moon, and the degree of the difference also makes a difference among three satellites. These differences can be interpreted as the presence of non-linearity: a meaningful quadratic term of a calibration equation. Based on the brightness of Venus and the moon, the correction of the albedo value is given by the following equations:

$$\begin{aligned} A' &= -0.1904A^2 + 1.7212A, \quad \text{GOES}-9 \\ A' &= -0.095A^2 + 1.7723A, \quad \text{GOES}-10 \\ A' &= -0.1691A^2 + 1.4847A, \quad \text{GOES}-12 \end{aligned} \qquad (3)$$

where

A': corrected albedo (post-launch calibrated albedo)

A: albedo calculated by GVAR counts with pre-launch calibration coefficients

These equations are diagrammed in Figure 12. Note that there is a possibility that the non-linearity is progressive, because the response of the visible channel must be linear before the launch. The time span of the data used in this study was just a half year, hence the long term trend of the non-linearity is unknown and will be investigated in future study.

Satellite	Venus	Moon	Venus / moon
9	0.630	0.587	1.073
10	0.583	0.567	1.028
12	0.748	0.682	1.097

Table 4. Ratio of Imager Sensitivity to Pre-launch Calibration in April 2004

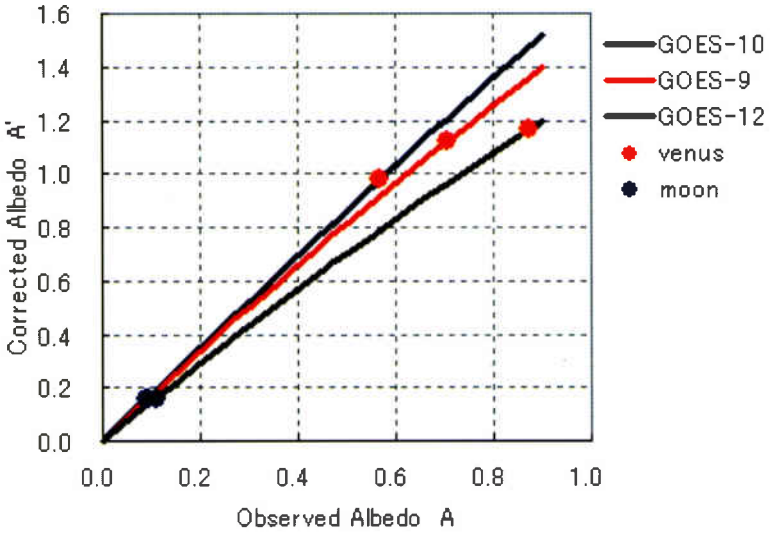

Figure 12. Albedo Correction Functions

The vertical axis of this figure indicates corrected albedo, and the horizontal axis shows the observed albedo that is computed by GVAR counts and the pre-launch calibration coefficients.

6. Verification

The above-mentioned visible channel calibration correction based on the brightness of Venus and the moon is verified here.

The observed lunar albedo shown in Tables 2 and 3 is verified by the brightness of Jupiter. The comparison of Jupiter's brightness is presented in Table 5. The measured lunar albedo is supported by Jupiter in consideration of unsettled clouds in the atmosphere of Jupiter, because lunar ratio: Cp/CL in Table 3, and Jupiter's ratio: O/C in Table 5 indicate close values.

The brightness of Venus is substantiated indirectly because of no proper brightness reference. In the case of Venus, meaningful error exists in both observed and predicted brightness. The observed brightness contains errors due to incomplete field-of-view measurement and interpolation in the non-oversampled North-South direction discussed in Section 3. The prediction of the brightness has

the error of the ephemeris itself and changing clouds. Since each imaging has different relative placement of Venus on a pixel lattice, the issue originated in the incomplete field of view and interpolation can be resolved. The effect of the Venusian clouds, that move very fast, must indicate a short cycle. Hence, the errors can be reduced by averaging brightness measurements, because most of these error sources can be interpreted as a random noise source. A key issue is a systematic error of the brightness.

Fortunately, a way to know the degree of the systematic error can be obtained by the presence of the moon at low albedo and the different degree of sensitivity degradation between two neighboring satellites: GOES-10 and 12. Figure 13 shows an index that can change with the degree of the systematic error of the predicted Venusian brightness. The left chart of Figure 13 illustrates the effect of the Venusian brightness error on the corrected albedo A'. If the Venusian brightness has a systematic error, the corrected albedo A' changes in the same ratio for both GOES-10 and 12. Since the brightness of Venus is different between GOES-10 and 12 due to the difference in size of the field of view, a difference in the curve of the corrected albedo A' between GOES-10 and 12 appears and increases with the albedo value. The difference of the curve causes the slope of distribution in the right chart of Figure 13, because the difference increases with an albedo value. As the slope of distribution increases with the magnitude of the systematic error on the Venusian brightness, the relation between the systematic brightness error of Venus and the slope value is established as shown in the bottom chart of Figure 13. Note that the slope is not zero when no systematic brightness error exists, as a quadratic sensitivity curve cannot be compensated perfectly by the quadratic albedo correction equation given in Eq. (3), that is, the functional inverse to a quadratic equation is not another quadratic equation.

Figure 14 shows a comparison of the earth scene at the middle longitude of two satellites at local noon. The condition of the middle longitude and its local noon was selected since the two satellites could be seen at the same zenith angle from a point of interest on the ground, and the separation angle between the sun and satellite is almost the same for the two satellites. The connection of the two images can be seen as a gap of brightness in the operational composite image, and a difference of brightness between the right and left sides of the operational composite image is distinct, while the corrected image shown in the bottom is brighter and almost seamless. The corrected images visualize the effect and validity of the correction.

Figure 15 shows a numerical comparison of the operational and corrected albedo on the images shown in Figure 14. It can be read from this figure that the ratio of GOES-10 albedo to GOES-12 (right graph) on the corrected image is almost 1.0 over the entire range of albedo, and its slope is about -0.011. This slope value is applied to Figure 13, and then it can lead to estimation of a few percent of the Venusian brightness error.

The trend of the visible channel sensitivity will be obtained from additional image data, including archival data in future studies. Many cases that will be processed will make feedback to improve the analysis technique shown here, thus reducing the estimation error and knowing it more precisely.

Satellite	Date	Time [UT]	Total brightness [albedo]		O / C	O / C mean
			Observed (O)	Predicted (C)		
12	02-27-2004	1715	1.002	1.412	0.710	0.703
12	03-05-2004	1645	1.006	1.416	0.710	
12	06-28-2004	0915	0.564	0.819	0.689	

Table 5. Comparison of Jupiter's Brightness

Total brightness is defined as a summation of the albedo values of each pixel. The prediction of the brightness is calculated by an ephemeris in the same way as for Venus.

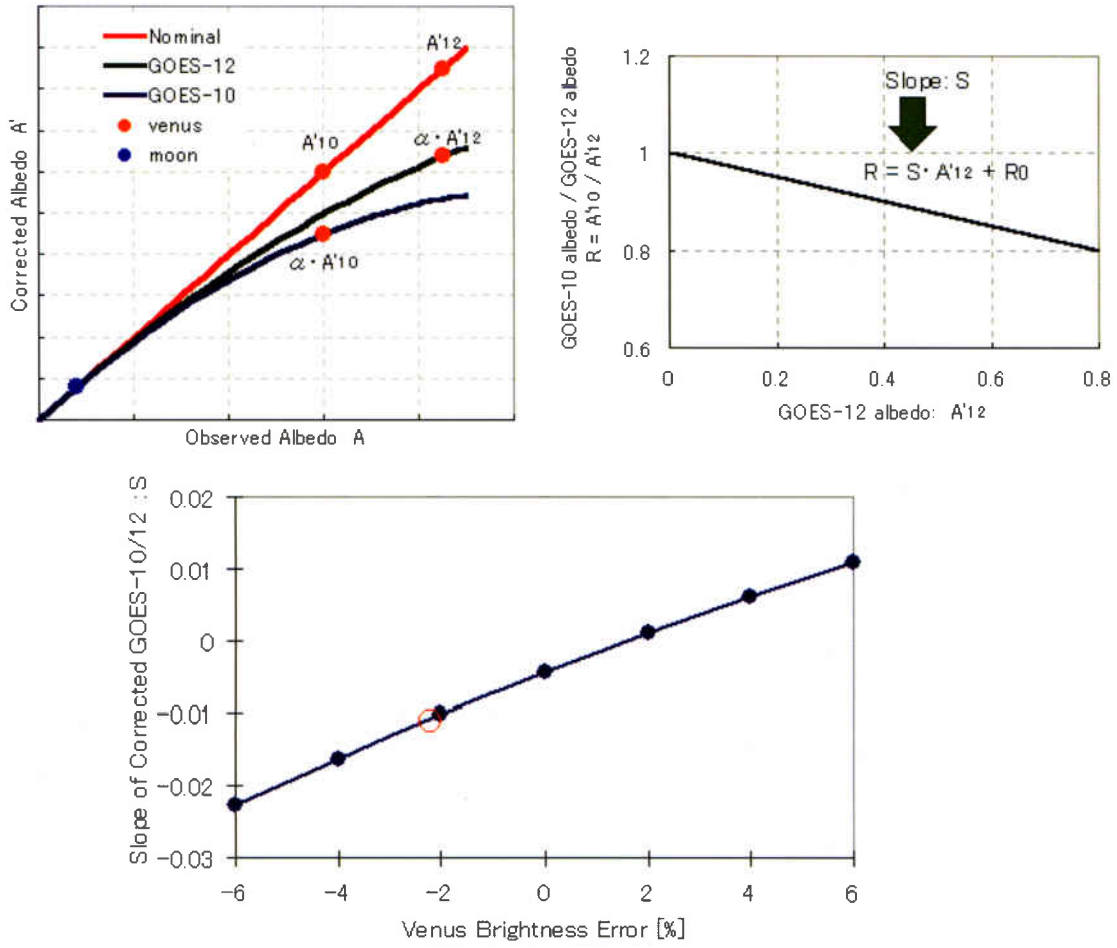

Figure 13. Estimation of Systematic Brightness Error of Venus

A red circle in the bottom chart indicates the measured slope shown in Figure 15.

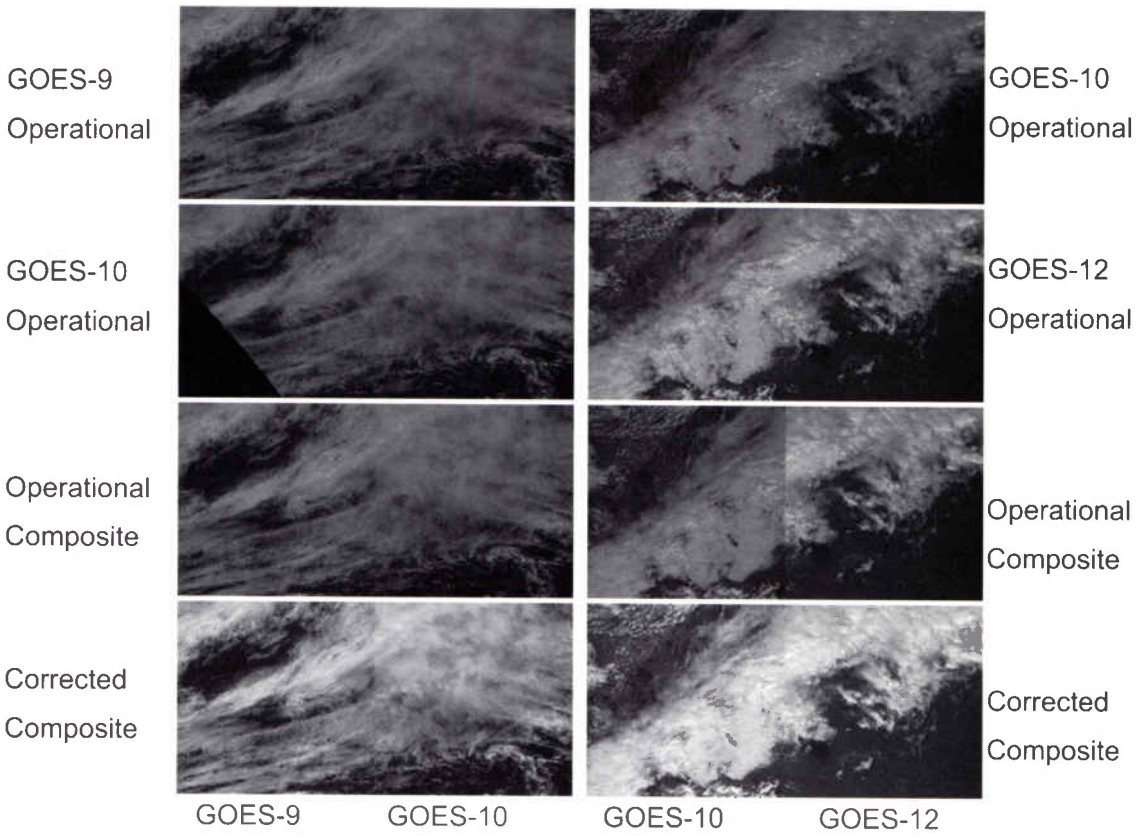

Figure 14. Visualization of Calibration Correction

The GOES-9/10 (left) composite was generated by images taken on September 5, 2004, 2330, and that of GOES-10/12 (right) by images on September 3, 2004, 1900. The clouds regain their brilliance in the corrected composites.

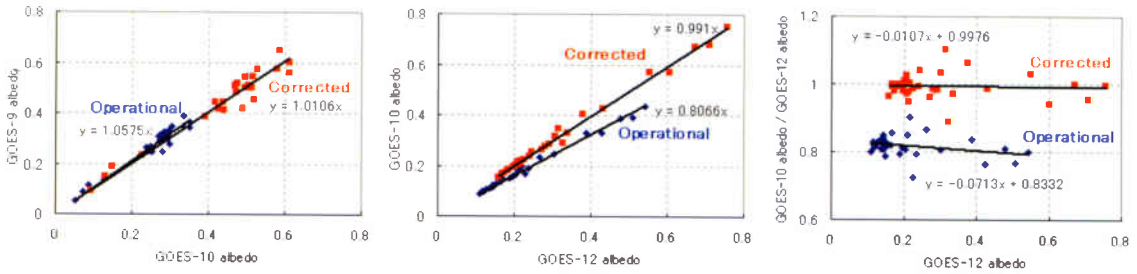

Figure 15. Comparison of Visible Imagery on GOES satellites

The mean values of one square degree (i.e., one latitudinal degree by one longitudinal degree) area from 27 to 50N at 170W for GOES-9/10, and from 19 to 50N at 105W for GOES-10/12, are plotted.

7. Conclusion

A new technique for the on-orbit visible channel calibration using Venus and the moon was developed. Venus works as a calibration reference at high albedo, and the moon at low. The Apollo 16 landing site on the moon was selected for the calibration reference because the laboratory-measured soil reflectance of the landing site is available. It was estimated that the sensitivity of the visible channel of GOES-9 Imager in April 2004 was 59 percent of the pre-launch measurement in the low albedo region. The non-linearity of the visible channel sensitivity was found, but its long-term trend is unknown. A correction algorithm of

an albedo value was developed, and its validity was demonstrated by Jupiter and the cloud brightness on the earth.

This newly developed technique can be applied not only to GOES imagers, but also to other satellites, including a spinner satellite. There is no need of a particular device in the instrument and special observation approach for this technique. Therefore, it should be a realistic task to re-calibrate the archival visible channel data. We may be able to trace the visible channel sensitivity back to 1974.

The visible channel calibration is becoming quantitative, using the above technique, to perform our mission: to deliver the best data to users.

The GOES-10 and GOES-12 Imager data used in this study was provided by the Comprehensive Large Array-data Stewardship System (CLASS) of NOAA, and GOES Project website of NASA/Goddard Space Flight Center.

References

----------, 2002: Rika nenpyo (Chronological Scientific Tables), National Astronomical Observatory (ed.), Maruzen Co., Ltd. (in Japanese)

Pieters, C. M., 1999: The Moon as a Special Calibration Standard Enabled by Lunar Samples: The Clementine Example (http://www.planetary.brown.edu/pds/Pieters_NV99_8025. pdf)

Chang, I-Lok, et al., 2004: Vicarious Calibration of GOES Imager Visible Channel: Use of Stars for Responsivity Trending (http://www.oso.noaa.gov/goes/goes-calibration/visible-channel.htm)

金星と月による GOES イメージャの可視チャンネル校正

木川　誠一郎*

要　　旨

金星は静止軌道から観測可能な最も明るい惑星である．金星の光度は金星上の雲による不確定性への懸念があるものの、画像取得装置の可視チャンネルの校正に適している．月は光度が低く、校正の有効範囲は反射率の低い領域に限定されるが、月には大気がなく安定した校正情報を提供する．

金星と月を用いた軌道上における可視チャンネル校正の新手法が開発された．金星と月はそれぞれ反射率の高い領域と低い領域において校正源として機能する．土壌反射率の実測値が存在するアポロ１６号の着陸地点が月における校正源として選定され、GOES-9 の低反射率領域では可視チャンネルの感度が打ち上げ前と比較して５９％であると推定された．可視チャンネルの感度に非直線性（つまり可視校正式の有意な２次の項）が発見された．これらの解析は木星の光度と地球の雲画像によって検証された．

* 気象衛星運用準備室